A Study on the Permeability Evolution of Self-Healing Mudstone Fracture Under Long-Term Stress

Hu Yunhao[1,2], Wu Jinxin[3], Dong Shuning[1,2], Yu Qingchun[3], Guo Xiaoming[1,2], Zhang Wenzhong[1,2], Zhang Xiyu[1,2]

[1]*Xi' an Research Institute of China Coal Technology and Engineering Group Corp, China, People's Republic of China*

[2]*State Key Laboratory of Coal Mine Hazard Prevention and Control, China, People's Republic of*

[3]*School of Water Resource and Environment, China University of Geosciences (Beijing), China, People's Republic of China*

Abstract

Self-healing capacity of roof aquitards in deeply buried coal seam goafs under long-term stress informs restoration strategies for damaged barriers. This work combines 260-day permeability tests on a mudstone fracture at 12 MPa confined pressure with fracture-scale COMSOL simulations. The decrease in permeability from transitions fast to slow. Early permeability declines rapidly due to channelization, bottlenecks, and electro-viscous effects. Dissolution–diffusion–precipitation processes and fines transport drive late-stage probable fluctuations and abrupt declines of fracture permeability. Under the tested conditions, the roof-water-region leakage barrier shows time-dependent self-healing, near-complete recovery within about three months after mining ends; late monitoring is also necessary.

Keywords: Deep-buried coal seam, mining-induced fracture, in-situ stress, water permeability, self-healing of aquiclude

Introduction

Northwest China harbors more than half of the nation's proven coal reserves, anchoring energy security for the country (Han *et al.* 2023). Yet this region is located in a dry to semi-arid climate where water resources are scarce, unevenly distributed, and groundwater system played a decisive supporting role in surface ecology (Liu *et al.* 2018). In deep goaf roofs, mining-induced disturbances fracture overburden strata, creating a water-conducting fractured zone. When these fracture networks intersect overlying aquifers, groundwater migrates toward the mined-out voids under gravity and hydraulic-head gradients, driving persistent underground inflows (Wang *et al.* 2019). Such inflows are not transient surges but long-lasting, self-healing–challenged losses that can persist for two to four years, yielding substantial groundwater depletion and ecological degradation (Yang *et al.* 2022). Remediation and reconstruction of damaged aquicludes thus emerge as essential components of sustainable, water-conscious coal development. A rigorous assessment of the self-healing capacity of damaged aquicludes under sustained formation stress is a prerequisite for deploying targeted restoration strategies with engineering precision.

Mudstone, a typical lithology of the aquiclude in the coal seam roof in the northwest coal mining area, has a high content of clay minerals and organic matter, and shows strong plasticity. Its permeability is highly sensitive to effective stress (Ju *et al.* 2020). Within geological sequences, mudstone thereby experiences prolonged, sustained stress, prompting progressive fracture closure and evolving permeability signatures. 30-day tests revealed pressure-solution and surface-erosion processes governing fracture permeability under elevated temperature (Cheng *et al.* 2021), while 60-day experiments showed rapid permeability reductions under a fixed confining pressure, with declines exceeding 90% within the first days and

continuing thereafter (Zhu and Yu 2024). Such short-duration studies inadequately capture long-term trajectories essential for engineering design and risk management, leaving a gap in understanding how mudstone fractures evolve under mining-relevant timescales.

To address this gap, we conducted permeability experiments on a single mudstone fracture for 260 days under a constant confining pressure of 12 MPa. Laboratory measurements were complemented by fracture-scale numerical simulations of water transport through the fracture. The experimental program, coupled with modeling, targets the coupled mechanical–chemical–particle-transport processes that govern self-healing under prolonged stress, with implications for roof-water-region governance and mine-water management.

Sample and Experiment

Mudstone core S1 was collected from the Anding Formation in the Ordos Basin, Northwest China at a depth of 762.6 m, yielding a dark-colored specimen. Cylindrical samples (25 mm diameter, 50 mm length) were prepared by wire-cutting. X-ray diffraction analysis identified quartz (46.8%) and clay minerals (48.5%) as the dominant phases. The water-saturated matrix permeability was measured as 2.59×10^{-18} m^2. A single longitudinal fracture was introduced at the core center using the Brazilian splitting method (Zhu and Yu 2024).

The experimental apparatus comprised a core holder, a confining-pressure loading system, a fluid-injection path, and a fluid-detection system. The core holder, with cushions at both ends, was enclosed in fluorinated rubber sleeves. A confining-pressure pump supplied water around the sleeves, with a central flow path linking the injection system to the mudstone core. Spiral grooves on the cushion cross-sections ensured uniform distribution of the injected fluid. A range of flow meters, depending on testing requirements, was employed; the instrument used in this study had a maximum full-scale of 0.5 mL and an accuracy of $\pm2.5\times10^{-3}$ mL, with a minimum range of 0.2 mL and an accuracy of $\pm1\times10^{-3}$ mL.

Saturation and permeability measurements followed a multi-step protocol. The sample was saturated in a high-pressure reactor with deionized water, using helium to pressurize the pore space to 15 MPa (Cheng and Yu 2019). Saturated samples were then placed in the core holder, and a confining pressure of 12 MPa was applied. Permeability was measured by the steady-state method (Yang *et al.* 2025). Water at 4 MPa inlet pressure was supplied, while the downstream outlet was vented to atmosphere; upon stabilization, the upstream–downstream pressure differential and flow rate were recorded synchronously to compute permeability. Each experimental set was repeated 2–3 times; individual measurement durations ranged from 2 to 6 h. If the relative deviation among measurements was ≤ 5%, the results were deemed reliable, and the mean value represented the steady-state flow rate. Matrix and fracture measurements followed the same operational protocol. Permeability generally varies with formation temperature and effective stress (Zhao *et al.* 2023); all experiments occurred in a temperature-controlled chamber with a constant temperature of 303.15 K and a confining pressure of 12 MPa to approximate deep formation conditions (Zhu *et al.* 2024). The calculation methods for matrix permeability, fracture permeability and hydraulic aperture were presented in Zhu and Yu (2024).

Simulation

Fracture flow was simulated in COMSOL Multiphysics using an initial fracture surface geometry derived from 3D surface scans. The scan data were digitized in Surfer, converting the surface into XYZ coordinates. A 3D model was constructed by embedding a rough fracture within a cylindrical rock body (25 mm diameter, 50 mm length). The computational domain was discretized into 737,229 elements, with a maximum element size of 1.33×10^{-3} m and a minimum element size of 2.51×10^{-4} m.

Boundary conditions mirrored the experimental setup. Permeability was highest along the fracture diagonal to represent the dominant flow path created by fracture roughness, while permeability was reduced

elsewhere to reflect channelized flow and aperture heterogeneity (Zhu and Yu 2024). Simulations proceeded after each adjustment to the fracture-permeability distribution until the numerically computed flow rate matched the experimental value, thereby inferring the internal fracture structure. Matrix and fracture domains employed distinct flow models. Matrix flow was described by Darcy's law:

$$\frac{\partial}{\partial t}(\epsilon_p \rho) + \nabla \cdot (\rho u) = Q_m \quad (1)$$

$$u = -\frac{k_m}{u_w} \nabla P \quad (2)$$

where ϵ_p is the porosity (-); ρ is fluid density(kg/m^3); u is Darcy velocity (m/s), and Q_m is a mass source term of matrix (kg/(m^3·s)), k_m is the matrix permeability (m^2). Fracture flow utilized a quadratic Forchheimer description to capture inertial effects in the rough channel:

$$D_h \frac{\partial}{\partial t}(\epsilon_p \rho) + \nabla_T (D_h \rho u) = D_h Q_m \quad (3)$$

$$-\nabla P = A Q_f + B Q_f^2 \quad (4)$$

$$A = \frac{u}{k_f w D_h}, B = \frac{\beta \rho}{w D_h^2} \quad (5)$$

where D_h is the hydraulic aperture (m); Q_f is a mass source term of fracture (kg/(m^3·s)), A is the viscous resistance coefficient (-), which dominant in laminar flow; B is the inertial resistance coefficient (-), which becomes important under turbulent or high-velocity conditions; and β is the Forchheimer coefficient (m^{-1}).

Results and Discussion

Temporal evolution of permeability and hydraulic aperture

Permeability and hydraulic aperture within mudstone fractures decline non-monotonically over 260 days under sustained in-situ stress (Fig. 1). The rapid-decline phase (0–21 days) exhibits the steepest reductions, followed by a slower sustained-decline phase (22–80 days), and a relatively stable phase (81–260 days) with only minor changes. Specifically, permeability and hydraulic aperture decrease by 39.7% and 63.7% during 0–21 days, by 18.0% and 18.5% during 22–80 days, and by 7.3% and 5.6% during 81–260 days, respectively. Despite continuous downward trends, changes after day 80 are modest, indicating near-equilibrium conditions for self-healing of the aquicludes in the roof of a goaf approximately three months after mining ceases. One plausible explanation is that the rapid and sustained declines reflect evolving fracture morphology and connectivity under stress, with subsequent stabilization governed by coupled mechanical and chemical processes.

Mechanistic interpretation by temporal phase

Rapid-decline phase (0–21 days). Mechanical creep and clay swelling drive the initial drop in permeability. Stress-driven contact-area evolution between fracture walls results in progressive fracture closing, consistent with stress concentration effects observed in clay-rich mudstones (Zhu *et al.* 2024). Water-

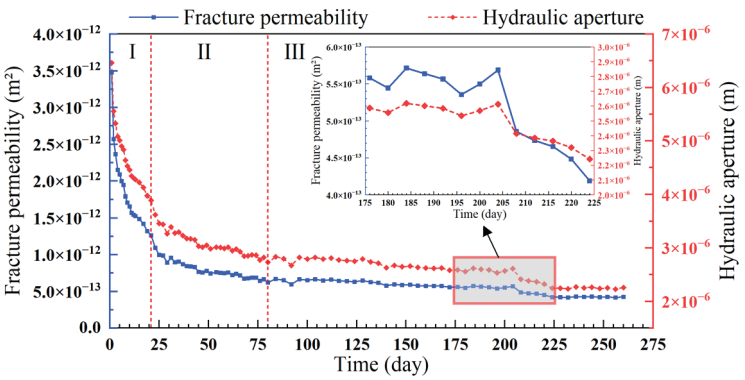

Figure 1 *The variation of water permeability in the fractured portions of the sample and the hydraulic aperture over time.*

induced clay swelling under saturation further augments closure, particularly within the early stage of exposure (van Noort and Yarushina 2019). These mechanisms collectively reduce flow pathways and enhance resistance to flow.

Sustained-decline phase (22–80 days). Flow becomes increasingly channelized within dominant fracture pathways. Bottlenecks controlling these channels dominate overall permeability; small reductions in bottleneck width yield disproportionate permeability decreases under confining stress. Water–mineral interactions also modulate transport: strongly adsorbed water can become immobile near mineral surfaces, reducing effective flow in constricted regions (Yang and Yu 2020). As stress continues, free water within wider segments diminishes, while narrower apertures compress toward the nanoscale. The narrowest bottlenecks increasingly govern transport. Electroviscous effects further suppress permeability by increasing flow resistance in these constrained regions (Li 2001).

Relatively stable phase (81–260 days). Sustained formation stress drives progressive contact-area growth between fracture surfaces, elevating fracture stiffness and rock strength while diminishing deformation capacity. The fracture approaches a new mechanical–chemical equilibrium. Persisting creep and mineral interactions yield minor fluctuations but no sustained deformation that would reopen flow paths. Permeability stabilizes as the system attains a balance among mechanical confinement, clay swelling, and dissolution–precipitation processes (Zhu and Yu 2024).

Abrupt late-stage decline (around day 205). An unforeseen, rapid drop ensues over roughly 20 days, surpassing prior trends (Fig. 1). The mechanism likely arises from the convergence of localized chemical and physical processes at fracture asperities under sustained 12 MPa confinement and flow (Huang *et al.* 2023). Asperities experience stresses well above the bulk level, elevating the chemical potential and initiating pressure solution of minerals (quartz and clays dominate the mudstone) at contact points, with dissolved material diffusing to lower-stress zones, precipitating elsewhere, or being flushed from the sample, so that dissolution–diffusion–precipitation (DDP) cycles progressively modify contact geometries and surface roughness (Sac-Morane *et al.* 2025). Concurrently, we consider that flow interacts with the rough fracture surfaces through scouring, liberating fines; these fines may deposit at bottlenecks to form bridge plugs or filter cakes that occlude channels, or be efficiently flushed to temporarily restore connectivity, yielding permeability fluctuations as the dominant pathways reorganize. The abrupt late-stage decline therefore reflects a coupled chemical–mechanical–particle-transport reconfiguration that cannot be captured by purely mechanical closure models; the observed perturbation emerges within the broader non-monotonic evolution—rapid creep and clay swelling during 0–21 days, followed by channelization-dominated reductions 22–80 days—when chemical mass transfer and fines dynamics progressively constrain flow and drive a sharp reorganization of the fracture-network permeability. This mechanism also explains discrepancies between observed trajectories and simplified simulations, underscoring the importance of incorporating DDP and fines transport in predictive models for mudstone fractures under sustained stress.

Fluid-transport dynamics from fracture-scale simulations: Simulations of fracture-flow under formation stress reveal pronounced channelization and flow reduction. Over a 120-day window, average fracture velocity declines from 0.213 m/s to 0.0202 m/s, a 90.6% decrease, signaling substantial compression, reduced effective flow area, and elevated flow resistance within the fracture network. In contrast, matrix flow remains orders of magnitude lower, near 10^{-7} m/s, and exhibits relatively small variation. During the initial compaction phase (first 12 days), dominant flow pathways contract rapidly; a limited set of channels persists and governs the fracture's bulk transport behavior. As stress persists, the initially small channels progressively close, while the originally large pathways continue to constrict and transform into smaller conduits; by day 80, flow is discernible only near those conduits that were originally large but have since narrowed to small apertures (Fig. 2).

Mechanistic synthesis and implications: One plausible explanation is that multiple processes operate in concert to produce the observed permeability evolution. In early stages, mechanical compaction and clay swelling dominate closure. In intermediate stages, flow preferentially follows a shrinking set of bottlenecks, with water–mineral interactions and electro-viscous effects further suppressing transport. In later stages, dissolution–diffusion–precipitation and pressure-solution mechanisms contribute to fluctuations in permeability by altering local mineralogy and roughness. The abrupt late-stage decline reflects a transient balance between scour-induced channel modification and fines deposition, temporarily enhancing or obstructing connectivity depending on particle transport efficiency.

Consequences for roof-water-region governance and mining practice: The non-monotonic evolution emphasizes that self-healing of mudstone fractures within deep coal-mining settings is time-dependent and path-sensitive. Short-term reductions in permeability may provide immediate leakage barriers, but long-term stability depends on sustained mechanical–chemical interactions and the fate of fines within bottlenecks. The approximately three-month timeframe for near-complete self-healing informs governance planning and strategies for water preservation in mining, enabling risk-aware design of roof-water-region protection. However, late-stage perturbations underscore the need for monitoring of fracture pathways and fines dynamics to prevent unanticipated permeability changes.

Conclusions

This study demonstrates a non-monotonic evolution of fracture permeability in mudstone under sustained in-situ stress, controlled by coupled mechanical, chemical, and particle-transport processes. In 260 days, permeability declines fastest in the rapid-decline phase (0–21 d) due to mechanical creep and clay swelling closing flow paths; a sustained-decline phase (22–80 d) is governed by channelization and bottlenecks, with water–mineral interactions and electro-viscous effects further suppressing transport; a relatively stable phase (81–260 d) approaches a new quasi-equilibrium. An abrupt late-stage decline around day 205 may reflects a synchronized reconfiguration driven by dissolution–diffusion–precipitation and fines dynamics that pure mechanical closure models cannot capture. Simulations of fracture-flow under formation stress

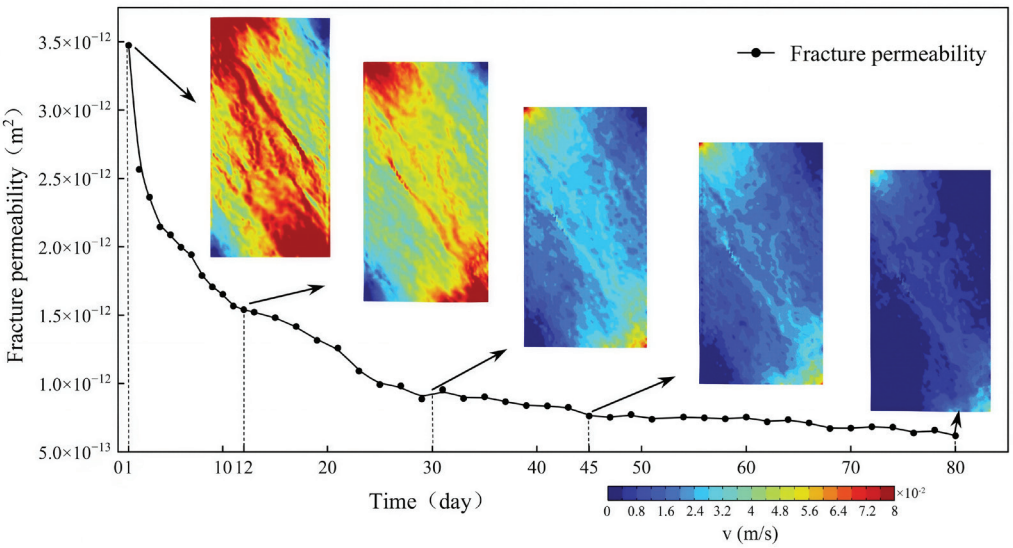

Figure 2 *Evolution of fracture permeability and the flow velocity field within the fracture during the initial 80-day experimental period (X-Y plane).*

reveal pronounced channelization and flow reduction. Practically, under the tested conditions, the roof-water-region leakage exhibits time-dependent self-healing, suggesting that it reaches its self-healing limit within about three months after mining ceases; nonetheless, late-stage late monitoring is also necessary. For modeling, incorporating DDP, fines transport, channelization, and electro-viscous effects is essential for reliable predictions. Our integrative framework clarifies the drivers of permeability trajectories and informs risk-aware strategies for roof-water-region protection. Future work should extend time scales, mineral diversity, and field-scale validation.

Acknowledgements

The authors thank all co-organisers for hosting the IMWA 2026 Conference. This study was funded by K Key Research and Development Program of Shaanxi (Program No. 2025SF-YBXM-510) and Tiandi Science and Technology Co. Ltd. Science and Technology Innovation Venture Capital Special Project (Grant No. 2025-TD-QZ030).

References

Cheng C, Herrmann J, Wagner B, Leiss B, Stammeier JA, Rybacki E, Milsch H (2021) Long-term evolution of fracture permeability in slate: an experimental study with implications for enhanced geothermal systems (EGS). Geosciences 11:443. https://doi.org/10.3390/geosciences11110443

Cheng P, Yu Q (2019) Experimental study on the relationship between the matric potential and methane breakthrough pressure of partially water-saturated shale fractures. J Hydrol 578:124044. https://doi.org/10.1016/j.jhydrol.2019.124044

Han Y, Wang Q, Li W, Yang Z, Gu T, Wang Z (2023) Predicting the height of the water-conducting fractured zone in fully mechanized top coal caving longwall mining of very thick jurassic coal seams in western China based on the NNBR model. Mine Water Environ 42:121–133. https://doi.org/10.1007/s10230-023-00918-6

Huang X, Kang Z, Zhao J, Wang G, Zhang H, Yang D (2023) Experimental investigation on micro-fracture evolution and fracture permeability of oil shale heated by water vapor. Energy 277:127677. https://doi.org/10.1016/j.energy.2023.127677

Ju J, Li Q, Xu J, Wang X, Lou J (2020) Self-healing effect of water-conducting fractures due to water-rock interactions in undermined rock strata and its mechanisms. Bull Eng Geol Environ 79:287–297. https://doi.org/10.1007/s10064-019-01550-x

Li D (2001) Electro-viscous effects on pressure-driven liquid flow in microchannels. Colloids Surf Physicochem Eng Asp 195:35–57. https://doi.org/10.1016/S0927-7757(01)00828-7

Liu S, Li W, Wang Q (2018) Height of the water-flowing fractured zone of the jurassic coal seam in northwestern China. Mine Water Environ 37:312–321. https://doi.org/10.1007/s10230-017-0501-1

Sac-Morane A, Rattez H, Veveakis M (2025) Importance of precipitation in the slowdown of creep behavior induced by pressure solution. J Eng Mech 151:04025025. https://doi.org/10.1061/JENMDT.EMENG-8360

van Noort R, Yarushina V (2019) Water, CO2 and argon permeabilities of intact and fractured shale cores under stress. Rock Mech Rock Eng 52:299–319. https://doi.org/10.1007/s00603-018-1609-8

Wang F, Xu J, Chen S, Ren M (2019) Method to predict the height of the water conducting fractured zone based on bearing structures in the overlying strata. Mine Water Environ 38:767–779. https://doi.org/10.1007/s10230-019-00638-w

Yang P, Yang W, Nie Y, Saleem F, Lu F, Ma R, Li R (2022) Predicting the height of the water-conducting fractured zone based on a multiple regression model and information entropy in the northern Ordos basin, china. Mine Water Environ 41:225–236. https://doi.org/10.1007/s10230-021-00805-y

Yang S, Yu J, Liu D, Li Y (2025) Effect of persulfate stimulation on matrix alteration and permeability enhancement of fractured shale: core-flooding experiments and numerical simulation. Gas Sci Eng 138:205612. https://doi.org/10.1016/j.jgsce.2025.205612

Yang S, Yu Q (2020) Experimental investigation on the movability of water in shale nanopores: a case study of carboniferous shale from the qaidam basin, china. Water Resour Res 56:e2019WR026973. https://doi.org/10.1029/2019WR026973

Zhao D, Chang H, Pu Y, Feng Z, Li X (2023) Study on mechanical parameters and creep seepage characteristics of different coal and rock combination samples. Geomech Geophys Geo-Energy Geo-Resour 9:25. https://doi.org/10.1007/s40948-023-00569-5

Zhu N, Cheng P, Yu Q (2024) Experimental study on the time-dependent gas permeability of fractures in shales. Rock Mech Rock Eng 57:695–718. https://doi.org/10.1007/s00603-023-03578-8

Zhu N, Yu Q (2024) Temporal evolution of fracture transport properties of fractured shales during long-term stress compaction. Eng Geol 339:107663. https://doi.org/10.1016/j.enggeo.2024.107663